Full metal wideband cosecant squared pattern antenna with a highly compact hybrid feed network

Lu, Yunlong; Huang, Mingjian; You, Qingchun; Xu, Lintong; Wang, Yi; Huang, Jifu

DOI:
10.1109/TAP.2022.3168713

Full Metal Wideband Cosecant Squared Pattern Antenna With a Highly Compact Hybrid Feed Network

Yunlong Lu, *Member, IEEE,* Mingjian Huang, Qingchun You, Lintong Xu, Yi Wang, *Senior Member, IEEE,* and Jifu Huang

***Abstract*— This paper presents a full metal wideband high-performance cosecant squared (CSC^2) pattern antenna. A highly compact structure is achieved by a convoluted feeding network routed in multiple layers. Double metal-ridges are added to the flared radiation slot to reduce the aperture size of the antenna element. A line of forty such elements are excited by a full-corporate feed network arranged longitudinally, so as to form a phased array in the future. A hybrid of single-ridge waveguide and coaxial line in a sandwich structure is used to construct the feed network. The absorbing wedge loaded coupler and magic-T are incorporated into the feed network to achieve high isolation and large power-division ratio, thereby improving the stability of the amplitude and phase distribution. This ensures the desired CSC^2 patterns over a wide frequency band. A prototype operating at C-band is designed, fabricated and measured. Experimental results show that the antenna has an impedance bandwidth ($|S_{11}|$<-13.1 dB) from 6 GHz to 7.4 GHz. Stable CSC^2 patterns in E-plane with the peak gain of over 16.5 dB and sidelobe level of less than -17.5 dB are observed across the same frequency band.**

Keywords—*Cosecant squared pattern antenna, wideband antenna, full metal structure, full-corporate feed network, waveguide coaxial line.*

I. Introduction

Antennas with cosecant squared (CSC^2) pattern can achieve an equal radiation power coverage within the required distance. In the CSC^2 region, the antenna gain gradually decreases with increasing elevation angles, so as to maintain the signal strength received in different areas [1]-[3]. In some specific scenarios, antennas with this pattern characteristic play an important role. For example, this allows 5G base stations to achieve specific field of view (FOV) coverage for optimal energy efficiency and low system complexity, and surveillance radars to detect approaching targets at a constant height [4]-[6].

A lot of efforts have been made to realize the CSC^2 pattern antennas [7]-[23]. Shaped reflector or reflectarray was firstly developed to achieve the CSC^2 pattern in a broadband [7]-[13]. In this type of antenna, the feed radiator needs to be accurately installed at a certain distance from the main radiator to obtain good illumination. This leads to a high profile and bulky volume. To overcome these shortcomings, planar antennas have been resorted to. Work has been reported based on microstrip line or substrate-integrated waveguide (SIW) [14]-[22]. Among them, most of the works adopt a series feed configuration to reduce antenna complexity and dielectric loss [16]-[22]. However, the series-fed fixed-beam antenna commonly suffers from narrow bandwidth. A SIW-based slot antenna with series-fed structure was reported in [20]. Its fractional bandwidth (FBW) with stable radiation patterns is only 1.4% (42.3-42.9 GHz). [21] presents a series-fed patch array antenna with a cosecant fourth power pattern. It achieves an FBW of 5% in the frequency range of 23.8- 25 GHz. Similarly, a series-fed patch array based on a SIW structure in [22] is employed to obtain the CSC^2 pattern. However, the achieved FBW is only 3.5%. For wideband wireless communication and radar applications, this narrowband characteristic is a significant limiting factor. In addition, the dielectric loss in the previous work is inevitable, which restricts from further improvement of antenna performance. [23] reported a slot array antenna with CSC^2 beam at 35 GHz. Air-filled waveguide was used to improve the antenna efficiency. However, the antenna is still series-fed, which limits its bandwidth. Due to the complexity and large occupied volumetric space of hollow-waveguide based full-corporate-feed network, it remains a challenge to achieve a wideband full metal CSC^2 pattern antenna with high performance within a compact footprint.

This paper aims to tackle this challenge. The proposed antenna has end-fire radiation pattern and a compact size along the antenna aperture plane, which makes it suitable for forming 1-D phased arrays. The main features of the proposed antenna are: (i) A double ridge loaded flared radiation slot, excited by a square coaxial line, is devised as an element to achieve compact size and good radiation performance over a wide frequency band. (ii) A full-corporate feed network based on a combination of single-ridge waveguide and square coaxial line is routed in

This work was supported partly by National Key R&D Program of China under Project 2018YFB1802100, in part by National Natural Science Foundation of China under Projects 62171242, 61801252, U1809203, and 61631012, in part by Zhejiang Natural Science Foundation under Project LY21F010002, Ningbo Natural Science Foundation under Project 202003N4108; and in part by the Fundamental Research Funds for the Provincial Universities of Zhejiang under Grant SJLY2020001. (*Corresponding author: Qingchun You, Jifu Huang.*)

Yunlong Lu, Mingjian Huang, Lintong Xu, and Jifu Huang are with the College of Electrical Engineering and Computer Sciences, Ningbo University, Ningbo, Zhejiang, 315211, China (e-mail: luyunlong@nbu.edu.cn).

Qingchun You, and Yi Wang are with School of Engineering, University of Birmingham, B15 2TT, United Kingdom (e-mail: y.wang.1@bham.ac.uk).

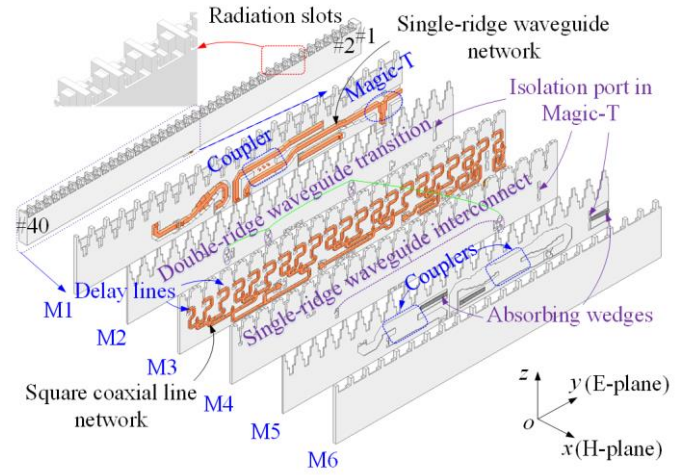

(a)

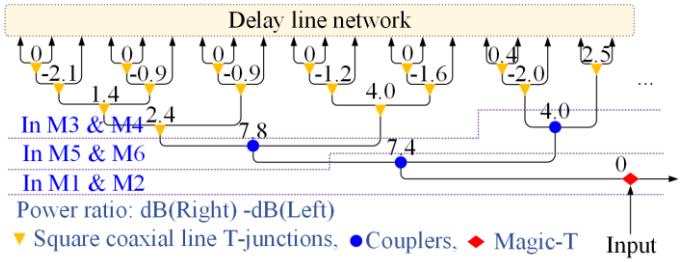

(b)

Fig. 1. Antenna configuration. (a) 3D view; (b) schematic of feed network.

TABLE I
TARGET SPECIFICATION OF THE CSC^2 PATTERN ANTENNA

Frequency band		6-7.4 GHz
Reflection coefficient		<-10 dB
Radiation patterns		End-fire
Polarization		Vertical
Beamwidths	E-plane (CSC^2 pattern)	30° @-20 dB
	H-plane	>90° @-3 dB
SLL in E-plane		<-20 dB
Peak gain		>16 dBi
Gain ripple in CSC^2 pattern region		<1.5 dB
Dimensions		1115 ×22×90 mm^3

multiple layers to meet the space constraint in array applications. (iii) Because of the requirements of large power-division ratio and amplitude/phase distribution stability in a wideband, absorbing wedge loaded couplers and magic-T are incorporated in the feed network. These features enable a wideband and stable CSC^2 pattern with a highly compact structure.

The paper is organized as follows: Section II describes the design of the array element. Section III and IV discuss the CSC^2 pattern synthesis and the corresponding antenna analysis and design. Section V gives the experimental validation followed by conclusion in Section VI.

II. ANTENNA CONFIGURATION

Fig. 1(a) shows the configuration of the proposed CSC^2 pattern antenna. It consists of the radiation part and a full-corporate feed network. An array of 40 flared slot elements arranged along the *y*-axis (E-plane direction) is excited by the feed network. The space between the adjacent elements should

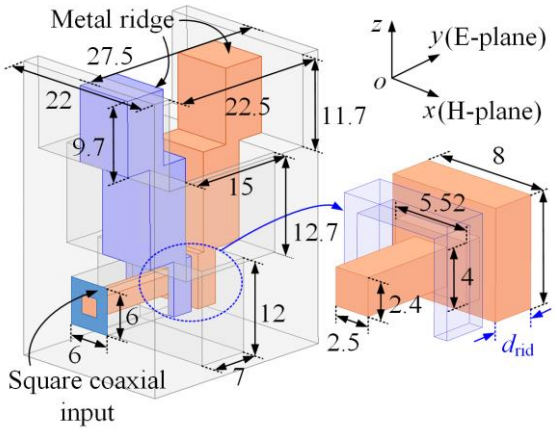

Fig. 2. Structure of radiation element. All dimensions are given in millimeter.

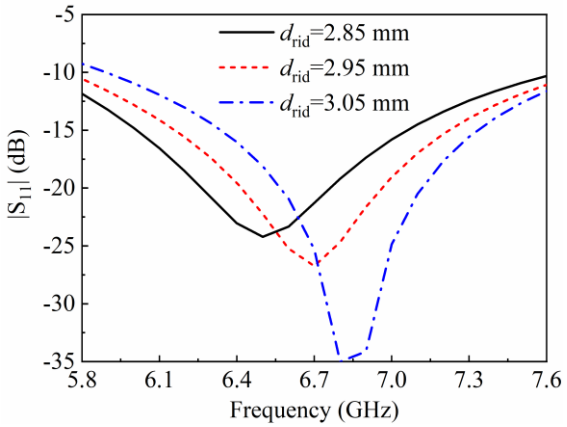

Fig. 3. Simulated reflection coefficient with different values of d_{rid}

be less than λ_H (λ_H is the free space wavelength at the highest operating frequency) to avoid grating lobes. In this work, the dimension of the radiation element in *x*-axis (H-plane direction) is restricted within 0.55 λ_H (corresponding to a beam scanning range of about ±55°). This will allow to build a phased array along H-plane in the future. The feed network consists of six couplers, one magic-T, multiple T-junctions, as well as the delay lines. To make a trade-off between the occupied space and the manufacture complexity, it uses a hybrid of single-ridge waveguides and square coaxial-lines, and folded in a sandwich structure with the single-ridge waveguide networks on the sides and the square coaxial-line network in the middle. The single-ridge waveguide circuit contains the six couplers and one Magic-T, located in Layers M1, M2, M5 and M6. The coaxial-line circuit is composed of multiple T-junctions and corresponding delay lines, located in Layers M3 and M4. Fig. 1(b) shows the circuit schematic of feed network. Considering the structural symmetry (the delay line part is anti-symmetrical, which is shown in Table II), only half of the feed network is presented. The layout of each layer of the circuit is presented in section III-B.

The feeding network should generate desired amplitude and phase distributions to ensure low sidelobe levels (SLL) and CSC^2 pattern in E-plane. Absorbing wedges are incorporated into the couplers and Magic-T to improve the amplitude and phase distributions. The single-ridge waveguide bend and the transition structure from the coaxial line to the single-ridge

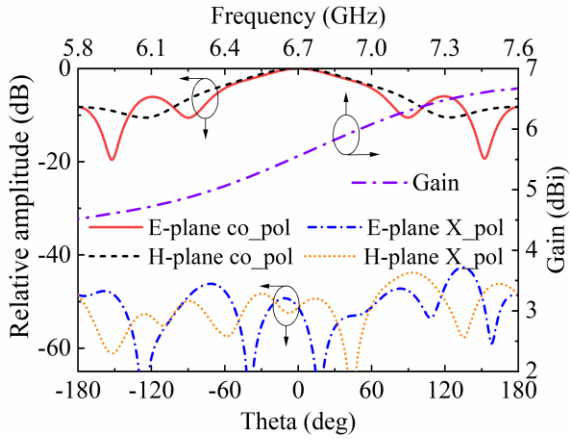

Fig. 4. Simulated radiation performance of one antenna element.

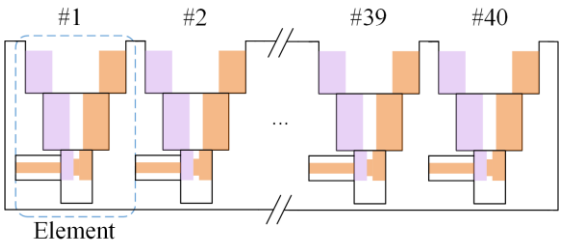

Fig. 5. Arrangement of the 40 antenna elements for CSC^2 pattern.

waveguide are used to interconnect signal paths between metal layers. The amplitude and phase response, as well as the implementation of the feed network, will also be discussed in section III-B. The frequency band of interest is 6-7.4 GHz (C-band), which is a common frequency band for surveillance radar applications. Other specifications of the proposed CSC^2 pattern antenna are tabulated in Table I. It is designed to achieve compact size, end-fire, and stable CSC^2 patterns in a wide frequency band. All the simulation results are carried out using Ansoft HFSS. The design and analysis of each block is presented in the following sections.

III. Design and Analysis

A. Radiation Part

Fig. 2 plots the structure of a radiation element. It is a flared slot and has end-fire radiation and vertical polarization characteristics. Considering the aforementioned phased array application in H-plane, the width of the radiation slot is 22 mm in this work (corresponding to 0.55 λ_H). The cut-off frequency of a hollow rectangular waveguide with this width (the width is larger than the height in the rectangular waveguide) is about 6.8 GHz, which cannot cover the whole operating frequency band. To decrease the cut-off frequency, two metal ridges are added in the flared radiation slot. An open-slot structure is adopted on the H-plane sides of the radiation slot. When building a phased array based on this unit, the radiation slots can be merged into a continuous transverse stub (CTS) slot for beam scanning [24], [25]. The size of the radiation slot along E-plane is set to 27.5 mm, which corresponds to 0.68 λ_H. Due to the strictly limited space, a square coaxial line is utilized to feed the radiation element, as it has a more compact size than the waveguide. An enlarged view of the feed structure is shown in Fig. 2. By

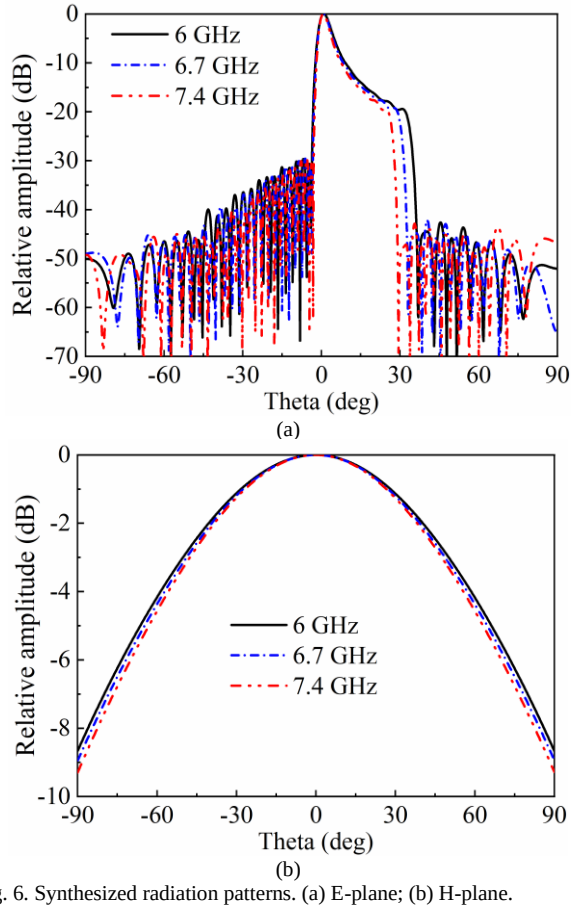

Fig. 6. Synthesized radiation patterns. (a) E-plane; (b) H-plane.

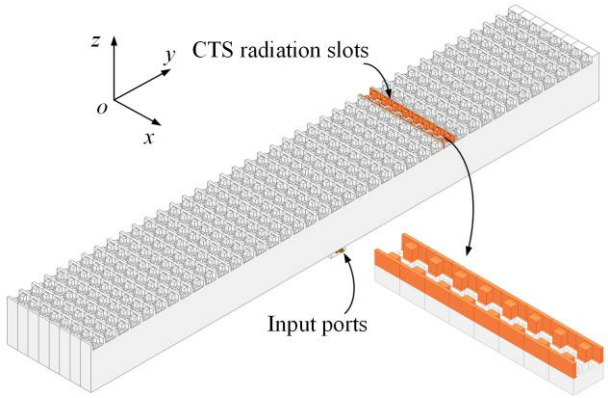

Fig. 7. Configuration of a 1-D phased array based on eight proposed constant squared pattern antennas.

adjusting the thickness (d_{rid}) of the metal ridge connecting the inner conductor of the coaxial line, the input impedance matching can be improved. Fig. 3 shows the simulated reflection coefficient with different values of d_{rid}. Other optimized dimensions are shown in Fig. 2. When d_{rid} = 2.95 mm, the optimal impedance matching is obtained with $|S_{11}|$<-10 dB over the frequency range of 5.8-7.6 GHz.

Fig. 4 illustrates the radiation performance of the element. The normalized radiation patterns are plotted at the center frequency of the operating band. The 3-dB beamwidths in E- and H-planes are 78° and 94°. The cross-polarization discrimination is better than 40 dB. Over the desired frequency range, the peak gain is over 4.7 dBi.

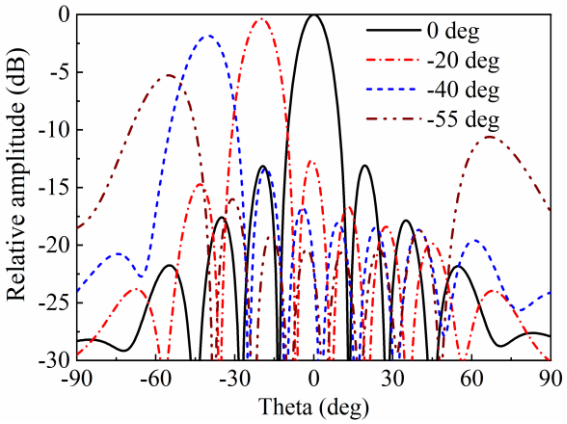

Fig. 8. Beam scanning performance in H-plane.

TABLE II
AMPLITUDE AND PHASE VALUES OF EXCITATION SIGNAL FOR DIFFERENT ELEMENTS

Element number	Amplitude (dB)	Phase (deg)	Element number	Amplitude (dB)	Phase (deg)
#1	-25.69	-85.1	#21	0	-13.9
#2	-25.69	-17.6	#22	-2.52	-36.2
#3	-24.81	3.3	#23	-6.2	-38.4
#4	-24.81	11.5	#24	-6.99	-30.3
#5	-24.81	11.1	#25	-7.45	-38.1
#6	-22.68	27.8	#26	-10.04	-41.8
#7	-20.09	22.5	#27	-11.43	-32.6
#8	-20.09	23.7	#28	-11.43	-35.8
#9	-17.96	35.8	#29	-13.77	-40.3
#10	-15.61	30.2	#30	-15.61	-30.2
#11	-15.61	30.2	#31	-15.61	-30.2
#12	-13.77	40.3	#32	-17.96	-35.8
#13	-11.43	35.8	#33	-20.09	-23.7
#14	-11.43	32.6	#34	-20.09	-22.5
#15	-10.04	41.8	#35	-22.68	-27.8
#16	-7.45	38.1	#36	-24.81	-11.1
#17	-6.99	30.3	#37	-24.81	-11.5
#18	-6.20	38.4	#38	-24.81	-3.3
#19	-2.52	36.2	#39	-25.69	17.6
#20	0	13.9	#40	-25.69	85.1

Forty antenna elements are arranged in a line along *y*-axis to achieve the low SLL CSC^2 pattern in E-plane, as shown in Fig. 5. The space between the adjacent elements is selected to equal to the element size along E-plane to realize the compactness of the whole antenna. Based on the above element performance and array space, the required amplitude and phase distributions for the CSC^2 pattern are obtained through optimization using the combination of discrete Fourier transform and genetic algorithm [26]. The discrete Fourier transform is first used to obtain initial amplitude and phase distributions that satisfy the CSC^2 pattern. Then, the SLL and gain ripple in the CSC^2 pattern region are optimized using the genetic algorithm. The optimal values of these amplitude and phase for each element are listed in Table II. It should be noted that these values are obtained at a SLL of -30 dB. There is a 10 dB margin between this and the target value (see in table I) to accommodate performance degradation from fabrication tolerance. Based on these values, the synthesis normalized radiation patterns at different frequencies are plotted in Fig. 6. It can be seen that in the frequency band of interest, the stable CSC^2 pattern with a gain ripple of less than 0.3 dB is achieve in E-plane. The SLL is suppressed by more than 29.5 dB. The 20-dB beamwidth in E-plane is about 30° and the 3-dB beamwidth in H-plane is around ±48° across the same frequency band.

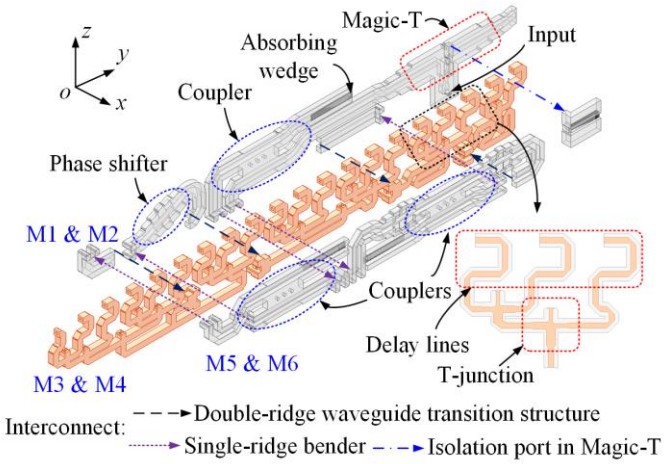

Fig. 9. Routing of half of the feed network.

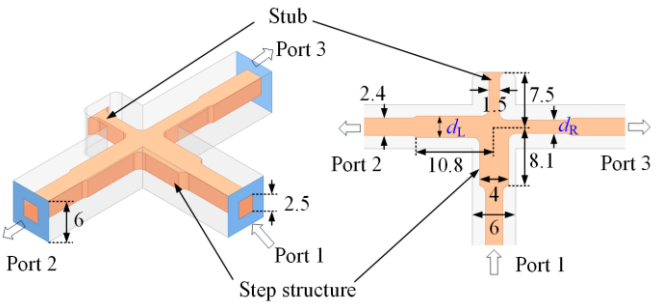

Fig. 10. Structure of the coaxial line T-junction. All dimensions are given in millimeter.

For 1-D phased array applications, eight CSC^2 pattern antennas are used to theoretically demonstrate its potential beam scanning performance in H-plane. Fig. 7 shows the configuration of phased array. As mentioned before, the radiation slots in *x*-axis are connected to form a CTS slot. Fig. 8 shows the simulated beam scanning performance at the highest frequency of 7.4 GHz. A wide scanning range of ±55° can be realized.

B. Feed Network

The feed network is realized as follows: First, design an unequal and in-phase power divider to obtain the desired amplitude distribution; then, cascade a delay line network to generate the phase distribution. The schematic of feed network is shown in Fig. 1(b). It is folded into a sandwich structure to reduce the antenna profile. The layout of each layer of the circuit and the signal interconnect are shown in Fig. 9. The coupler and magic-T help achieve large power-division ratios and high isolation to improve the stability of the desired amplitude and phase distributions. The required power-division ratio of each unequal power division unit is also indicated in Fig. 1(b). Noted that only half of the feed network is shown both in Fig. 1(b) and Fig. 9.

1) Square coaxial line circuits

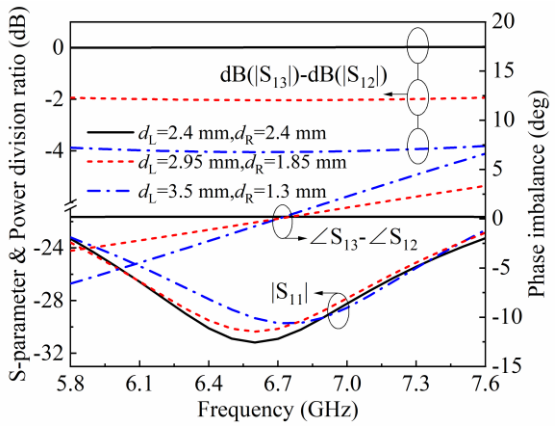

Fig. 11. Simulated amplitude and phase responses of the coaxial line T-junction.

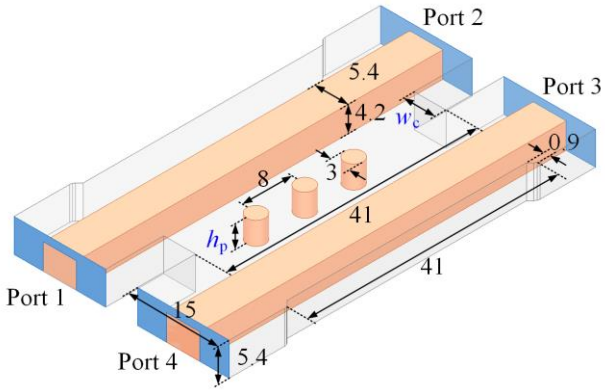

Fig. 12. Structure of the single-ridge waveguide coupler. All dimensions are given in millimeter.

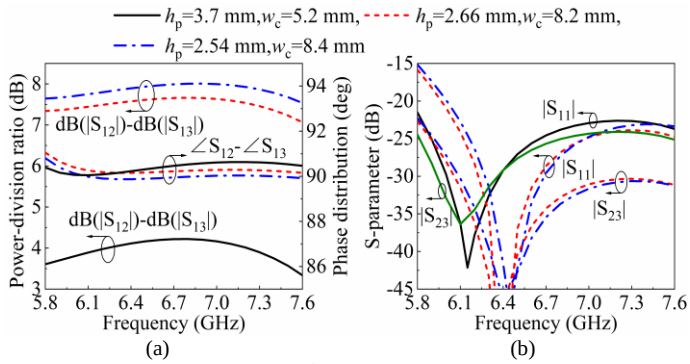

Fig. 13. Parameter analysis of single-ridge waveguide coupler. (a) Power-division ratio and phase imbalance; (b) S-parameters.

Half of the square coaxial line circuits includes a 4-to-20 power divider and corresponding delay lines. The 4-to-20 power divider, exhibiting in-phase response, consists of 16 T-junctions with different power-division ratios. To fix the coaxial signal line (center conductor), short-circuit stubs are added at the center of T-junctions. The basic stub-loaded coaxial line T-junction is shown in Fig. 10. Since the short-circuit stub is electrically short, its influence on the T-junction can be ignored [27], [28]. By adjusting the sizes of the output branch coaxial lines, the output power-division ratio can be controlled. Fig. 11 plots the simulated power-division ratios and phase imbalances with different dimensions of branch coaxial line. Obviously, the desired power-division

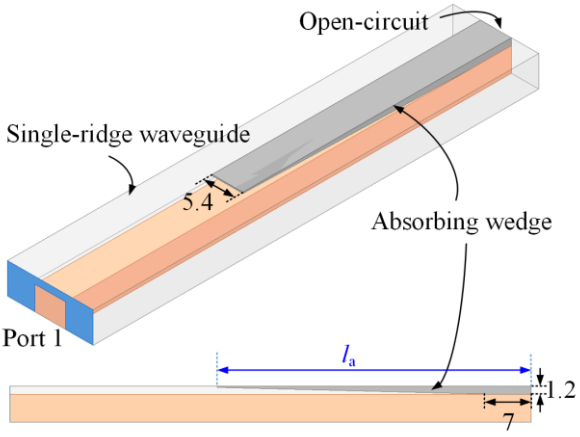

Fig. 14. Structure of absorbing wedge loaded in the single-ridge waveguide. All dimensions are given in millimeter.

ratios from 0 dB to 4 dB can be easily achieved. However, as the power-division ratio increases, the phase balance between the output ports deteriorates. This is compensated by adjusting the path length of the output signals, thereby ensuring the in-phase response of whole 4-to-20 power divider. The delay lines with different lengths are all bent into a U-shape to reduce size and obtain the desired phase distribution. The length for each delay line is determined at 6.7 GHz according to the specific values of the phase distribution (shown in Table II).

2) Single-ridge waveguide part

The single-ridge waveguide circuit is on both sides of the sandwich structure. One side is a coupler and a magic-T, and the other side is two couplers. The three couplers have different power-division ratio of 7.4 dB, 7.8 dB, and 4.0 dB with phase difference of 90° between the output ports. The structure of the 90° coupler, as well as the optimized dimensions, is shown in Fig. 12. The different power-division ratio is achieved by adjusting the height (h_p) of metal pins and width (w_c) of coupling region. Fig. 13 shows the simulated results of the corresponding parameter analysis. It can be seen that a large variation of power-division ratio from 4 to 7.8 dB can be obtained by using different combination of h_p and w_c, while maintaining an output phase difference within the range of 90°±1.2°. At the same time, a good impedance matching of $|S_{11}|$<-22.6 dB and a high isolation of over 24 dB between the output ports (Ports 2 and 3) are also achieved.

There is limited space to terminate the isolated port (Port 4) of the coupler with a 50 Ω connector. Thus, in this work, an absorbing wedge is used as the load and inserted into the single-ridge waveguide of Port 4 to obtain high-isolation. The absorbing material comes from Zhejiang Luchuang Material Technology Co., LTD, and its electromagnetic (EM) energy absorption at 8.6 GHz exceeds 60 dB when the length is 10 mm [29]. The shape and dimension of the absorbing wedge added in the single-ridge waveguide is presented in Fig. 14. By optimizing the length of wedge (l_a) inserted in the single-ridge waveguide, a good power division and a high isolation can be guaranteed. Fig. 15 plots the simulated reflection coefficient of absorbing wedge with different wedge lengths. It is noted that one end of the single-ridge waveguide is open-circuit. When l_a= 47 mm, the optimal $|S_{11}|$ of lower than -22.5 dB is obtained in

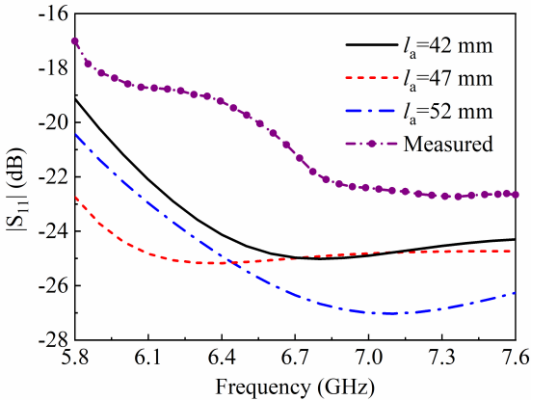

Fig. 15. Simulated reflection coefficients of absorbing wedge loaded single-ridge waveguide with different wedge lengths.

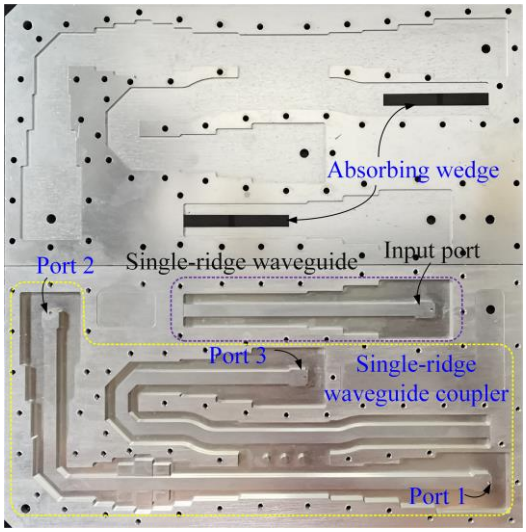

Fig. 16. Photograph of the fabricated single-ridge waveguide coupler with power-division ratio of 4.0 dB.

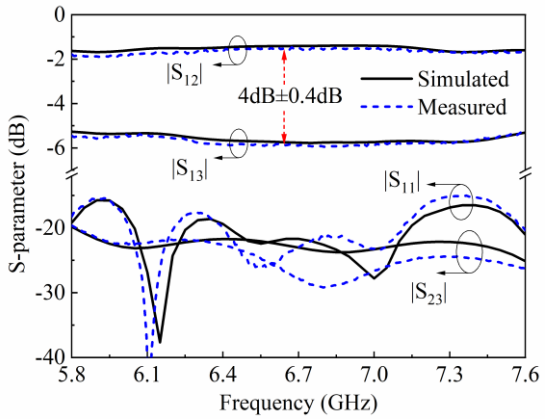

Fig. 17. Simulated and measured S-parameters of the fabricated coupler.

the frequency range of 5.8 – 7.6 GHz, showing a high EM-field energy absorption. For validation, a prototype is fabricated and measured. The photograph is shown in Fig. 16, and the measured result is also plotted in Fig. 15. Agilent E8361C network analyzer is used to perform the measured result. The measured $|S_{11}|$ is about 6 dB higher than the simulated one, mainly due to the small material parameter difference between the simulated models of the absorbing material and the actual one. Still it realizes an EM-field energy absorption of more than

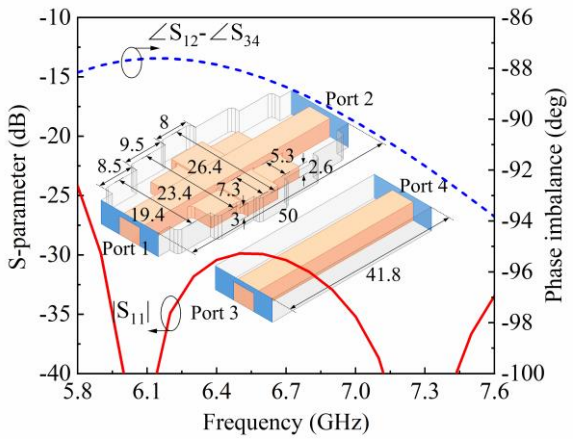

Fig. 18. Structure of the jagged single ridge waveguide phase shifter and simulated results. All dimensions are given in millimeter.

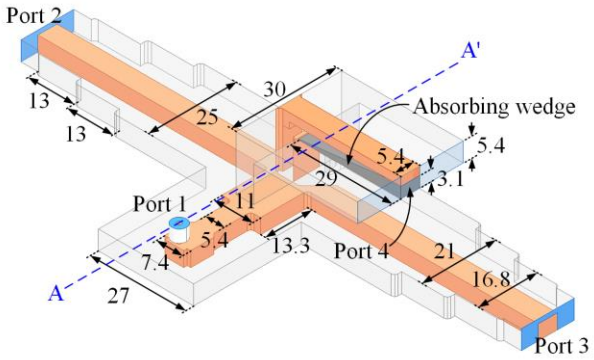

Fig. 19. Structure of the single-ridge waveguide Magic-T at the input. All dimensions are given in millimeter.

18.5 dB. An absorbing wedge loaded coupler with a power-division ratio of 4.0 dB is also fabricated and measured. The photograph of the fabricated coupler is shown in Fig. 16. Fig. 17 plots the simulated and measured S-parameters of the coupler. The simulation agrees well with the measurement, which proves the effectiveness of the absorbing wedge in this work. The measured reflection coefficient for each port is less than -15 dB in the frequency range of 6 – 7.4 GHz. The measured power-division ratio is 4.0 ± 0.4 dB and the measured isolation is over 22 dB. For the other two couplers with power-division ratios of 7.4 dB and 7.8 dB, the wedge lengths are also selected to be 47 mm.

In order to compensate the 90° phase difference between the output ports of the coupler, a 90° phase shifter is cascaded with the output ports of each coupler. Jagged waveguides have been proven in phase shifters [30], [31]. In this design, the jagged single-ridge waveguide structure is used. The structure and the simulated phase response are illustrated in Fig. 18. A 90°±2.7° phase shift is obtained in the desired frequency range.

At the antenna input, a Magic-T is employed to achieve the high isolation, in-phase and equal power division in the operating frequency band. The structure of the single-ridge waveguide Magic-T is shown in Fig. 19. The signal from Port 1 is divided into two paths to Port 2 and Port 3. Port 4 works as an isolation port. Similar to the coupler, an absorbing wedge with a length of 29 mm is inserted into the isolation port as a load. Due to the requirement of geometry symmetry of the Magic-T

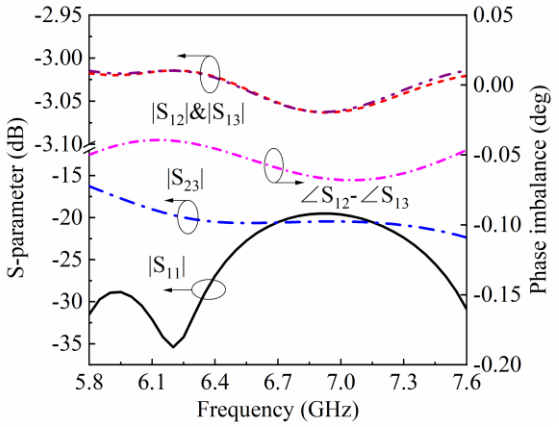

Fig. 20. Simulated amplitude and phase responses of the Magic-T.

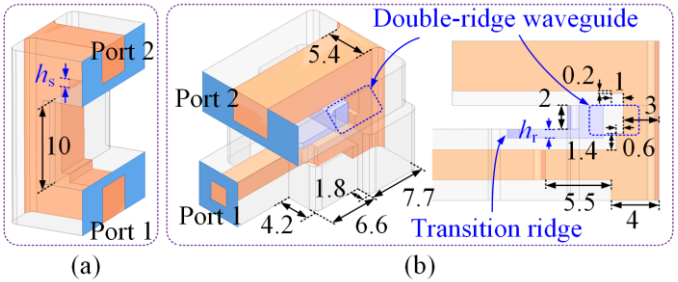

Fig. 21. Interconnect structures among the different layers of the sandwich structure. (a) Single-ridge waveguide bend; (b) double-ridge transition structure. All dimensions are given in millimeter.

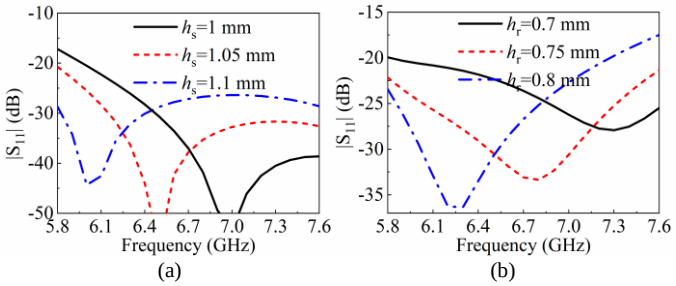

Fig. 22. Parameter analysis of the interconnect structures. (a) Single-ridge waveguide bend; (b) double-ridge waveguide transition structure.

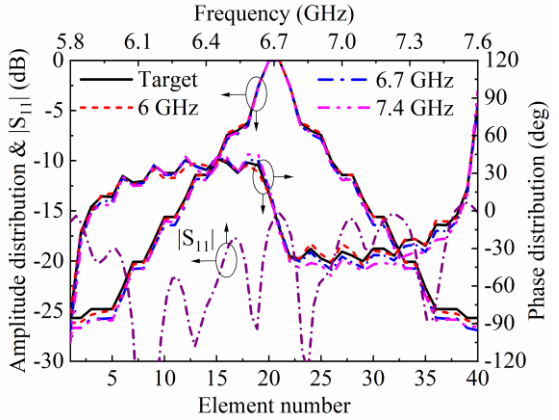

Fig. 23. Simulated $|S_{11}|$ of the whole feed network and the generated amplitude and phase distribution among the radiation elements.

along the A-A' plane, Port 4 should be implemented with a double-ridge waveguide structure for equal power division and in-phase characteristics. However, considering the shape and

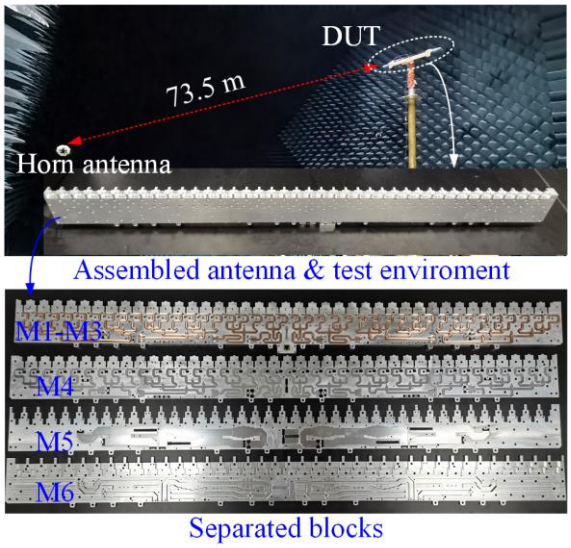

Fig. 24. Photographs of fabricated prototype and test environment.

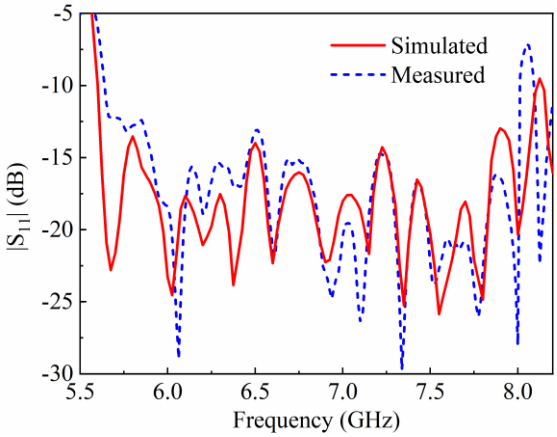

Fig. 25. Simulated and measured reflection coefficients of the CSC[2] pattern antenna.

installation of the absorbing wedge, the double-ridge waveguide in the path to the Port 4 is converted to the single-ridge waveguide. The design details of the conversion structure can be founded in [32], and not repeat here. Port 4 is bent 90° and laid out on the other side of the sandwich structure (as shown in Figs. 9 and 19). A coaxial connector is used as the standard input port to feed the antenna. Fig. 20. Shows the simulated amplitude and phase responses of the absorbing wedge loaded Magic-T. An in-phase equal power division and high-isolation is realized.

3) Interconnect structures

Ten single-ridge benders and eight transition structures of double-ridge waveguide are employed to support the signal interconnect among the different layers of the sandwich structure. Half of the single-ridge waveguide benders and double-ridge waveguide transition structures, as well as the interconnect relationship are shown in Fig. 9. The basic single-ridge waveguide bender and the single-ridge waveguide transition structure are shown in Fig. 21. Two steps are added in the corners on both sides of the bender to reduce the reflection caused by the waveguide discontinuities. This can be done by adjusting the height of the step (h_s). Fig. 22(a) shows the

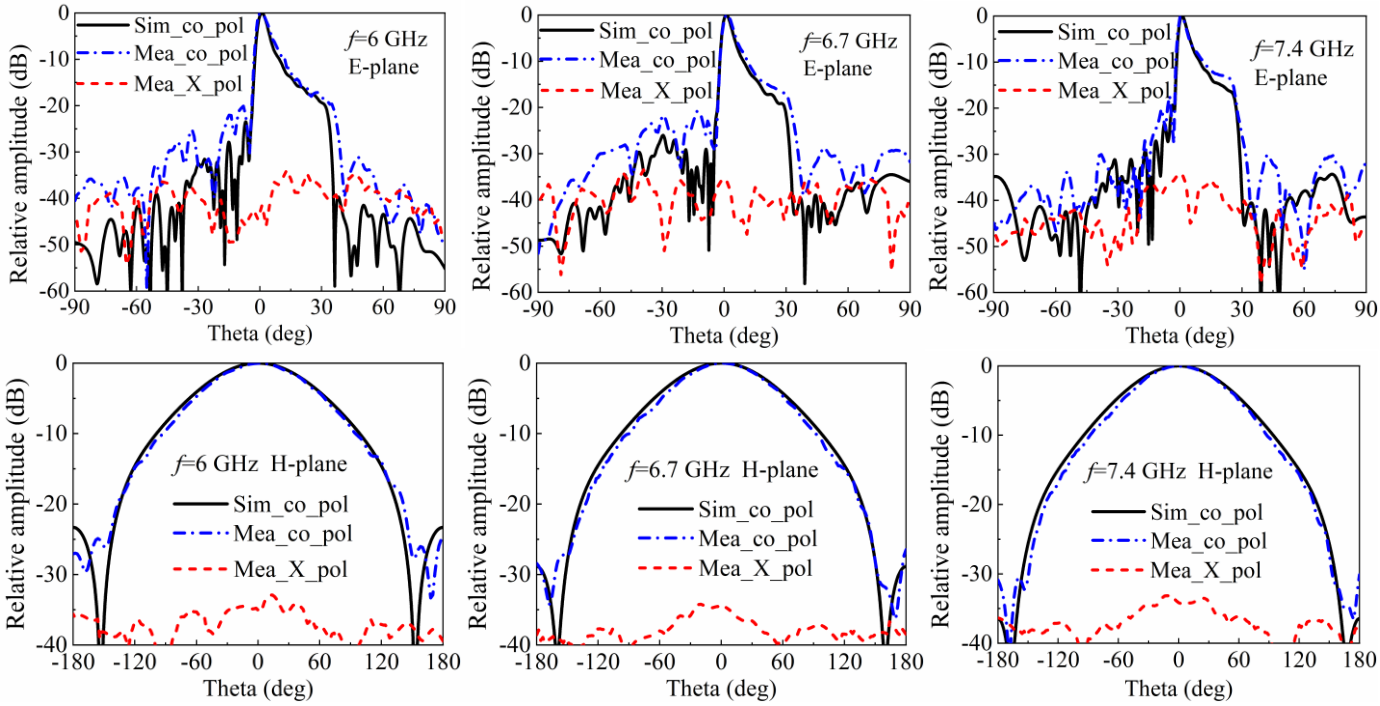

Fig. 26. Simulated and measured radiation patterns in E- and H-plane at different frequencies: (a) 6 GHz; (b) 6.7 GHz; (c) 7.4 GHz.

simulated S-parameters with different values of h_s. An optimal reflection coefficient of lower than -25 dB in the frequency range of 6.0-7.4 GHz is achieved when h_s= 1.05 mm.

A double-ridge waveguide is used to transit between the single-ridge waveguide and the square coaxial line. By adjusting the height (h_r) of the transition ridge in the double-ridge waveguide, the impedance matching in the operating frequency band can be improved. Fig. 22(b) shows the parameter analysis of metal ridge height. When h_r= 0.75 mm, the impedance matching with $|S_{11}|$<-23.5 dB can be obtained.

The simulated reflection coefficient of the whole feed network is shown in Fig. 23. In 6 -7.4 GHz, the $|S_{11}|$ remains below -15.5 dB, exhibiting a good input impedance matching. The calculated and simulated amplitude and phase distributions at different frequencies from the whole feed network to excite the radiation elements are also presented in Fig. 23. The results obtained from the feed network are in a good agreement with the desired ideal values. The largest deviation in amplitude and phase is within 1.2 dB and 13°, which occurs at 7.4 GHz. This ensures that a stable CSC^2 pattern can be realized in the operating frequency band.

IV. Experimental Results

The antenna is formed of six metal layers (M1-M6, shown in Fig. 1) and fabricated by milling using aluminum. Plenty of tightening screws around the signal path are used to assemble the prototype and suppress the leakage. The photographs of the assembled antenna, test environment and individual metal blocks are shown in Fig. 24. The size of the prototype is 1115 mm × 22 mm × 90 mm. the radiation performance is tested using far-field antenna test system.

A. Reflection Coefficient

Fig. 25 shows the simulated and measured reflection coefficient of the proposed CSC^2 pattern antenna. They are in a good agreement. The measured result is slightly higher than the simulated one, which is mainly attributed to the manufacturing tolerance and assemble errors. Over the frequency range of 6-7.4 GHz (fractional bandwidth of 20.9%), the measured $|S_{11}|$ is less than -13.1 dB.

B. Radiation patterns and Gain

The simulated and measured radiation patterns in E- and H-planes at different frequencies of 6 GHz, 6.7 GHz and 7.4 GHz are plotted in Fig. 26. The measured radiation pattern envelope of the main beam is in good agreement with the simulation. The measured 20-dB beamwdith in E-plane is larger than 32.2° over the desired frequency range of 6.0-7.4 GHz, wheareas the measured 3-dB beamwidth in H-plane is over 95°. The measured ripples in the CSC^2 pattern region is less than 1 dB, exhibiting a stable CSC^2 pattern in a wide frequency band. All these items satify the design target, given in Table I. The measured sidelobe pattern is higher than the simulated pattern in the E-plane. The meaured maximum SLL is -17.5 dB at 7.4 GHz, which is about 2 dB higher than the simulated one. This simulated SLL at 7.4 GHz is slightly higher than the design target (-20 dB), because the phase distribution generated by the feed network at this frequency has a relatively large deviation from the calculated value, as shown in Fig. 23. The incease in the measured SLL is mainly due to the deterioration of the generated amplitude and phase distributions among the radiation elements caused by multiple factors, such as manufacturing tolerances, assembly errors, and differences between the simulation and actual models of the absorbing material. The measured cross polarization patterns are also

TABLE III
PERFORMANCE COMPARISONS BETWEEN THE PROPOSED AND OTHER PUBLISHED WORKS

Ref.	Antenna type	Number of slots	Center frequency (GHz)/ FBW	Gain (dBi)	20-dB beamwidth	Gain ripple (dB)	SLL (dB)
[18]	SIW LWA	--	15.2/4.7%	>2	--	--	--
[19]	Slotted SIW	15×22	15/6.5%	>27.4	>60°	--	<-20
[20]	Slotted SIW	12	42.6/1.4%	>17.7	>45°	--	<-16.5
[21]	SIW fed patch array	6×12	24.4/5%	<20.4	>50°	--	<-14
[22]	Slotted SIW	16×16	28.5/3.5%	>14.3	~50°	<2.5	<-13
This work	Slotted HW	40×1	6.7/20.9%	>16.5	>30°	<1	<-17.5

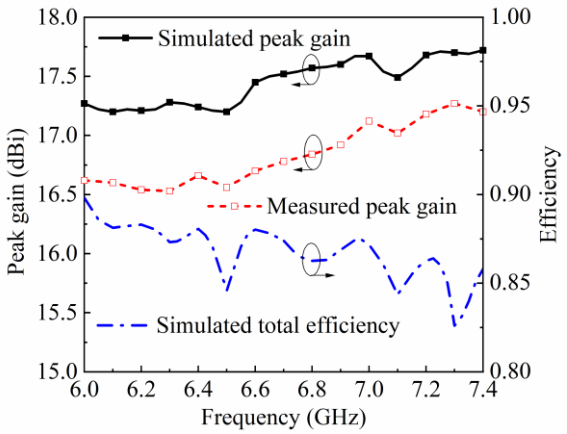

Fig. 27. Simulated and measured peak gain.

presented in Fig. 26. The cross polarization discrimination is better than 33 dB both in E- and H-planes.

The simulated and measured peak gain is plotted in Fig. 27. It varies from 16.5 dBi to 17.3 dBi in the frequency range of 6.0-7.4 GHz, while the simulated one is 17.2-17.7 dBi. The small difference is believed to be due to the manufacturing tolerance, assemble and test errors, as well as the power leakage at the interfaces between the metal layers. The simulated antenna efficiency is higher than 81% over the same frequency range.

C. Comparison

Table III compares this work with several other CSC^2 pattern antennas. All the compared antennas are based on microstrip line or SIW. The dielectric loss limits the antenna performance. Moreover, all these works employ series-fed structure. This makes the antenna bandwidth narrow. To the best of authors' knowledge, this is the first time a hollow-waveguide based full-corporate feed CSC^2 pattern antenna is reported. This antenna has a compact size, high antenna efficiency, low SLLs and stable CSC^2 patterns in a wide frequency band.

V. CONCLUSION

This paper demonstrates a wideband full-corporate feed CSC^2 pattern antenna. The size of the antenna along the H-plane is designed to be very compact ($0.55\lambda_H$), so that it can be suited to form phased arrays. The feed network, composed of a hybrid circuit based on single-ridge waveguide and square coaxial line, is folded into a sandwich structure to further reduce the antenna profile. Absorbing wedge loaded couplers and magic-T are incorporated into the feed network to generate the desired amplitude and phase distributions, so as to achieve a stable CSC^2 pattern in a wide frequency band. The prototype operating at C-band is designed, fabricated and measured. Simulation agrees well with the measurement, validating the design concept. The peak gains of over 16.5 dBi, gain ripples of less than 1 dB in the CSC^2 pattern region and SLL of lower than 17.3 dB are achieved across the frequency range of 6-7.4 GHz. The features of wideband and high radiation performance make this antenna an attractive candidate for radar and base station applications.

REFERENCES

[1] F. Scattone, M. Ettorre, B. Eddo, R. Sauleau and N. J. G. Fonseca, "Truncated leaky-wave antenna with cosecant-squared radiation pattern," *IEEE Antennas Wireless Propag. Lett.*, vol. 17, no. 5, pp. 841-844, May 2018.

[2] A. Dastranj, H. Abiri, and A. Mallahzadeh, "Design of a broadband cosecant squared pattern reflector antenna using IWO algorithm," *IEEE Trans. Antennas Propag.*, vol. 61, no. 7, pp. 3895–3900, Jul. 2013.

[3] A. Foudazi and A. R. Mallahzadeh, "Pattern synthesis for multi-feed reflector antennas using invasive weed optimisation," *IET Microw., Antennas Propag.*, vol. 6, no. 14, pp. 1583–1589, Nov. 2012.

[4] J. Puskely, Y. Aslan, A. Roederer, and A. Yarovoy, "SIW based antenna array with power equalization in elevation plane for 5G base stations," in *Proc. 12th EuCAP*, London, UK, Apr. 2018.

[5] K. Pandey, "Design of a cosecant square-shaped beam pattern SAR antenna array fed with square coaxial feeder network," in *Proc. 43th European Microwave Conference*, Nuremberg, Germany, pp. 1699-1702, 2013.

[6] M. Koubeissi, L. Freytag, C. Decroze and T. Monediere, "Design of a cosecant-squared pattern antenna fed by a new butler matrix topology for base station at 42 GHz," *IEEE Antennas Wireless Propag. Lett.*, vol. 7, pp. 354-357, 2008

[7] O. Yurduseven and O. Yurduseven, "Compact parabolic reflector antenna design with cosecant-squared radiation pattern," in *Proc. Microw., Radar Remote Sens. Symp. (MRRS)*, Aug. 2011, pp. 382–385.

[8] E. Carrasco, M. Barba, J. A. Encinar, M. Arrebola, F. Rossi, and A. Freni, "Design, manufacture and test of a low-cost shaped-beam reflectarray using a single layer of varying-sized printed dipoles," *IEEE Trans. Antennas Propag.*, vol. 61, no. 6, pp. 3077-3085, Jun. 2013.

[9] M. Arrebola, J. A. Encinar, and M. Barba, "Multifed printed reflectarray with three simultaneous shaped beams for LMDS central station antenna," *IEEE Trans. Antennas Propag.*, vol. 56, no. 6, pp. 1518-1527, Jun. 2008.

[10] A. Zeitler, J. Lanteri, C. Pichot, C. Migliaccio, P. Feil, and W. Menz, "Folded reflectarrays with shaped beam pattern for foreign object debris detection on runways," *IEEE Trans. Antennas Propag.*, vol. 58, no. 9, pp. 3065–3068, Sep. 2010.

[11] K. Henderson and N. Ghalichechian, "Triangular and rectangular lattices for cosecant-squared shaped beam reflectarrays," *IEEE Antennas Wireless Propag. Lett.*, vol. 20, no. 10, pp. 2058-2062, Oct. 2021.

[12] M. Milijić, A. D. Nešić, and B. Milovanović, "Design, realization, and measurements of a corner reflector printed antenna array with cosecant squared-shaped beam pattern," *IEEE Antennas Wirel. Propag. Lett.*, vol. 15, pp. 421-424, Jun. 2015.

[13] G. Carluccio, A. Mazzinghi and A. Freni, "Design and manufacture of cosecant-squared complementary reflectarrays for low-cost applications,"

IEEE Antennas Wirel. Propag. Lett., vol. 65, no. 10, pp. 5220-5227, Oct. 2017.

[14] J. Lei, G. Fu, L. Yang, and D. M. Fu, "Wide band linear printed antenna array with low sidelobe cosecant square-shaped beam pattern," *Prog. Electromagn. Res. C*, vol. 15, pp. 233-241, 2010.

[15] A. Kedar, P. N. S. Kutiyal, M. Garg, and U. K. Revankar, "Wide band low profile linear microstrip antenna array with cosecant square-shaped beam pattern," *Microw. Opt. Technol. Lett.*, vol. 49, no. 4, pp. 963-965, Apr. 2007.

[16] J. Hirokawa, C. Yamazaki, and M. Ando, "Postwall waveguide slot array with cosecant radiation pattern and null filling for base station antennas in local multidistributed systems," *Radio Sci.*, vol. 38, no. 2, Dec. 2002.

[17] H. Qi, F. Zhao, L. Qiu, K. Xiao, and S. Chai, "Design of a feed network for cosecant squared beam based on suspended stripline," in *Proc. Int. Symp. Antennas Propag.*, 2013, pp. 1005–1007.

[18] Y. Geng, J. Wang, Z. Li, Y. Li, M. Chen and Z. Zhang, "A leaky-wave antenna array with beam-formed radiation pattern for application in a confined space," *IEEE Access*, vol. 7, pp. 86367-86373, 2019.

[19] H. Chu, P. Li and Y. Guo, "A beam-shaping feeding network in series configuration for antenna array with cosecant-square pattern and low sidelobes," *IEEE Antennas Wirel. Propag. Lett.*, vol. 18, no. 4, pp. 742-746, Apr. 2019.

[20] Z.-C. Hao and M. He, "Developing millimeter-wave planar antenna with a cosecant squared pattern," *IEEE Trans. Antennas Propag.*, vol. 65, no. 10, pp. 5565–5570, Oct. 2017.

[21] Y. Yu, Z. H. Jiang, H. Zhang, Z. Zhang and W. Hong, "A low-profile beamforming patch array with a cosecant fourth power pattern for millimeter-wave synthetic aperture radar applications," *IEEE Trans. Antennas Propag.*, vol. 68, no. 9, pp. 6486-6496, Sep. 2020.

[22] J. Puskely, T. Mikulasek, Y. Aslan, A. Roederer and A. Yarovoy, "5G SIW based phased antenna array with cosecant-squared shape pattern," *IEEE Trans. Antennas Propag.*, vol. 70, no. 1, pp. 250-259, Jan. 2022.

[23] Y. J. Cheng, H. R. Zhang, Y. F. Wu, H. N. Yang and M. H. Zhao, "A proactive conformal waveguide slot array antenna with cosecant square beam," in *Cross Strait Radio Science & Wireless Technology Conference (CSRSWTC)*, Fuzhou, China, pp. 1-3, 2020.

[24] Y. You, Y. Lu, Q. You, Y. Wang, J. Huang and M. J. Lancaster, "Millimeter-wave high-gain frequency-scanned antenna based on waveguide continuous transverse stubs," *IEEE Trans. Antennas Propag.*, vol. 66, no. 11, pp. 6370-6375, Nov. 2018.

[25] F. Foglia Manzillo et al., "A wide-angle scanning switched-beam antenna system in LTCC technology with high beam crossing levels for V-band communications," *IEEE Trans. Antennas Propag.*, vol. 67, no. 1, pp. 541-553, Jan. 2019.

[26] G. Z. Guo and Y. Bing, "Antenna pattern synthesis of shaped-beam using a new combined algorithm," in Proceedings Asia-Pacific Conference on Antennas and Propagation, Harbin, China, 2014, pp. 291-293.

[27] M. Sano, J. Hirokawa and M. Ando, "A hollow rectangular coaxial line for slot array applications fabricated by diffusion bonding of laminated thin metal plates," *IEEE Trans. Antennas Propag.*, vol. 61, no. 4, pp. 1810-1815, Apr. 2013.

[28] M. Sano, J. Hirokawa and M. Ando, "Single-layer corporate-feed slot array in the 60-GHz band using hollow rectangular coaxial lines," *IEEE Trans. Antennas Propag.*, vol. 62, no. 10, pp. 5068-5076, Oct. 2014.

[29] [Online]. Available: http://www.xibopian.com/Product/8432104257.html

[30] Y. J. Cheng, W. Hong and K. Wu, "Broadband self-compensating phase shifter combining delay line and equal-length unequal-width phaser," *IEEE Trans. Microw. Theory Techn.*, vol. 58, no. 1, pp. 203-210, Jan. 2010.

[31] L. Polo-López, J. Córcoles, J. A. Ruiz-Cruz, J. R. Montejo-Garai and J. M. Rebollar, "Triple-radiation pattern monopulse horn feed with compact single-layer comparator network," *IEEE Trans. Antennas Propag.*, vol. 69, no. 5, pp. 2546-2559, May 2021.

[32] H. Zhao et al., "E-band full corporate-feed 32 × 32 slot array antenna with simplified assembly," *IEEE Antennas Wirel. Propag. Lett.*, vol. 20, no. 4, pp. 518-522, Apr. 2021.